RAA 2020 Vol. **20** No. **5**, 71(11pp) doi: 10.1088/1674–4527/20/5/71

http://www.raa-journal.org *http://iopscience.iop.org/raa*

***R**esearch in*
***A**stronomy and*
***A**strophysics*

Development of wideband orthomode transducers for FAST cryogenic receiver system

Jin Fan[1], Kai Zhu[1], Heng-Qian Gan[1], Peng Jiang[1], Jian Yang[2], Yang Cao[1], Hong-Fei Liu[1], Hang Zhang[1], Ming-Lei Guo[1] and Xiang-Wei Shi[1]

[1] CAS Key Laboratory of FAST, the National Astronomical Observatories, Chinese Academy of Sciences, Beijing 100101, China; *pjiang@nao.cas.cn; zhukai@nao.cas.cn; ghq@nao.cas.cn*

[2] Department of Electrical Engineering Antenna Group and the Department of Earth and Space Sciences [Onsala Space Observatory], Chalmers University of Technology, Gothenburg, Sweden

Received 2019 August 23; accepted 2019 September 21

Abstract This paper describes the design, construction, and performance of the wideband orthomode transducers (OMTs) for the L- (1.2–1.8 GHz), the S- (2–3 GHz) and the P- (0.56–1.12 GHz) band receiver systems of the Five-hundred-meter Aperture Spherical radio Telescope (FAST). These OMTs operate at the cryogenic temperature of 70 K to reduce their thermal noise contribution to the receiver chains. The development on the FAST L- and S-band quad-ridged waveguide (QRWG) OMTs is carried out based on the theoretical mode analysis. In view of the miniaturization of FAST cryogenic receiver system at P-band, a novel wideband compact bowtie dipole OMT is designed with an octave bandwidth as well as a length of only quarter wavelength. The proposed L-, S- and P-band OMTs are designed and optimized by using Ansys High Frequency Structure Simulator (HFSS), and then manufactured, tested at room temperature. Measurement of FAST cryogenic receiver system noise is also performed with the L-, S- and P-band OMTs installed. The measured results fully comply with the design specifications.

Key words: FAST — instruments — telescopes

1 INTRODUCTION

The Five-hundred-meter Aperture Spherical radio Telescope (FAST) has been built in a karst depression in Guizhou Province of southwest China with the goal of science focusing on the neutral hydrogen line surveying in distant galaxies out to very large redshifts, looking for the first shining star, detecting thousands of new pulsars, etc. (Nan 2006).

Seven sets of receivers are equipped ranging from 0.07–3 GHz and among them are three sets of cryogenic receiver systems covering a frequency range of L-band (1.2–1.8 GHz), S-band (2–3 GHz) and P-band (0.56–1.12 GHz). The block diagram of the cryogenic receiver front-end is shown in Figure 1. The feed horn efficiently converts propagating electromagnetic field near the reflector's focal point to a guided wave in the waveguide, followed by the orthomode transducer (OMT) which separates two orthogonal modes in the waveguide into two transmission lines in the same frequency band. A directional coupler is used to inject noise for system calibration and measurement. Low-noise amplifiers (LNAs) can amplify the signal and set the receiver noise level, and are followed by isolators, filters and additional amplifiers. Some of the key front-end receiver components [OMT, directional couplers, and LNAs] are housed inside a compact cryostat and cooled at a cryogenic temperature to reduce the system noise. The cryostat consists of a two-stage cryogenic cooler with nominal temperatures of 70 K and 25 K respectively and it is constrained by the limited space available inside the focal cabin of FAST, which requires a very compact design of all components of the receiver chain, particularly the OMTs which largely determine the size and weight of the dewar.

OMTs are critical passive components in both radio astronomy and telecommunication systems. Several different broadband OMT types have been presented, including the coupled waveguide (Boifot 1990; Reck & Chattopadhyay 2013), the planar (Grimes et al. 2007), the finline (Robertson 1956; Skinner & James 1991), and quad-ridged waveguide (QRWG) types (Skinner & James 1991; Coutts & M. 2011; Villiers et al. 2008;

Stennes 2000). For radio astronomy applications, the OMTs with low cross-polarization, low ohmic loss, and good impedance matching over a wide band are needed. The coupled waveguide OMT (Reck & Chattopadhyay 2013) has a simple structure and low reflection coefficient, but the bandwidth is limited, not more than 1.4:1, by the single-mode bandwidth in the waveguide. The planar OMT (Grimes et al. 2007) applies differential excitation that can broaden the single mode bandwidth to a value of 1.6:1 but two 180° hybrids and supporting dielectric substrates are needed, which leads to additional loss and therefore increases the noise. The finline OMT (Robertson 1956) has a wide bandwidth of 1.7:1 but its asymmetric structure results in a high cross-polarization level. The QRWG OMT (Skinner & James 1991; Coutts & M. 2011) has a wide bandwidth up to 2.2:1 with an excellently comprehensive performance and symmetrical structure but usually requires 2.4–4 low-frequency wavelengths (Villiers et al. 2008) not suitable for applications below 1 GHz.

In this paper, we aim at developing wideband OMTs for FAST L-, S- and P-band Cryogenic Receiver Systems. The main technical specifications for L-band antenna system are the sensitivity of A/T 1500 m^2 K^{-1} and T_{sys} around 25 K. The targeted frequency bandwidth range for FAST L-, S- and P-band receivers are 1.2–1.8 GHz, 2–3 GHz and 0.56–1.12 GHz, respectively, with return loss better than –15 dB and cross-polarized isolation more than 30 dB for the OMTs. Moreover, it is required the OMTs have a low ohmic loss so low noise temperature can be achieved. Design scheme and development of the wideband orthomode transducer for L-, S- and P-band will be elaborated in the following sections.

2 DEVELOPMENT OF FAST QRWG OMTS AT L- AND S- BAND

Several QRWG OMTs have shown excellently comprehensive performance: low cross-polarization couplings, low ohmic loss and wide impedance bandwidth. It was selected as a candidate for FAST cryogenic OMTs operating above 1 GHz (L-band and S-band).

2.1 FAST QRWG OMT Structure

The structure of the QRWG OMTs for FAST L- and S-band cryogenic receiver systems is shown in Figure 2(a). This QRWG OMT is based on a circular waveguide with the same diameter as the corrugated horn waveguide, so no transitions connecting different aperture planes is needed (Fan et al. 2017). The circular QRWG is fed by two coaxial lines through the ridges, with the inner conductors connected to the corresponding opposite ridges, similar to the structure in Skinner & James (1991) and Stennes (2000). At the shorting end, the quadruple ridges is terminated with a sunken conical cavity, different from the convex one in Skinner & James (1991) to decrease the length. The tops of the ridges are in the shape of a 45-degree ridge chamfer with a flat surface in the center (shown in Fig. 3(a)), different form V-shape ridges in Skinner & James (1991) and Stennes (2000), so that irregular in-band trapped mode will not be introduced. The design of the profile of the ridges is presented in the next subsection.

2.2 Design Procedure

QRWG OMTs can be divided into two sections for analysis as shown in Figures 2(b) and 2(c). The first section is the coaxial to constant cross-sectional quad-ridged waveguide transition. The next is the tapered quad-ridged to circular waveguide transition. The QRWG OMT can be designed in three steps:

1. Design of coaxial to quad-ridged waveguide transition.

2. Design of smooth transition from the quad-ridged to the circular waveguide transition.

3. Electrical performance optimization of integral OMT structure.

Since no closed-form solution exists for analyzing the quad-ridged shape, the analysis of coaxial to quad-ridged waveguide transition and quad-ridged to circular waveguide along the tapered transition as well as the integral OMT optimization are carried out using Ansys High Frequency Structure Simulator (HFSS).

2.2.1 Design of coaxial to quad-ridged waveguide transition

Important design parameters of coaxial to quad-ridged waveguide transition include the diameter of the circular waveguide, the thickness of the ridge t, the gap width between opposing ridges in the throat section g (see Fig. 3(a)), and the position of the feed point of the coaxial probe. The selection of parameters t and g is determined according to mechanical feasibility, as well as to ensure mode and input impedance properties.

The propagation constants of TE11 mode and TE21L mode in the QRWG with different gap width g are calculated in Figure 4. The dotted lines are propagation constant curves of TE11 mode versus frequency with different gap width values of g and the solid lines correspond to TE21L mode. When the propagation constant drops to zero, the mode is cut-off at that frequency. It can be seen that with the increase of gap width g from 6 mm to 150 mm, the cut-off frequency of TE11 mode increases from 0.2 GHz to 0.9 GHz, while the cut-off frequency of TE21L waveguide does not change significantly. In fact, the radius of the

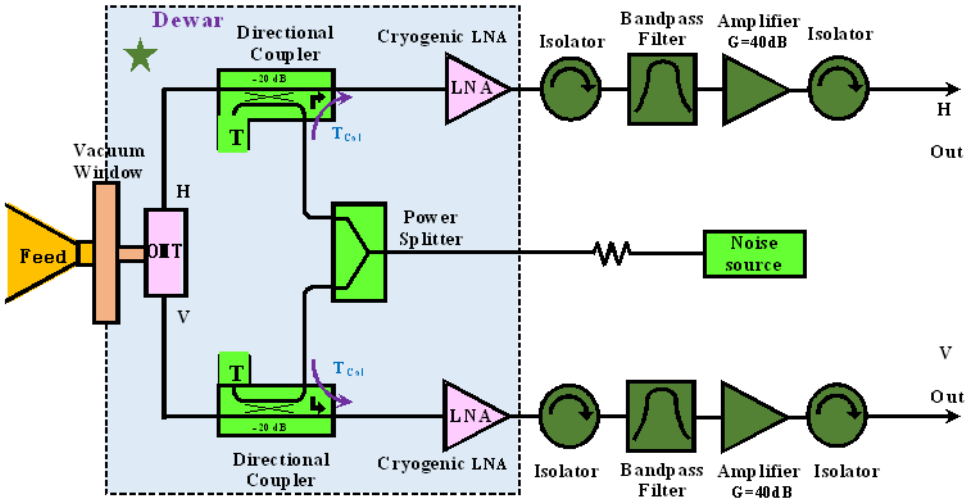

Fig. 1 The block diagram of front-end of FAST cryogenic receiver system.

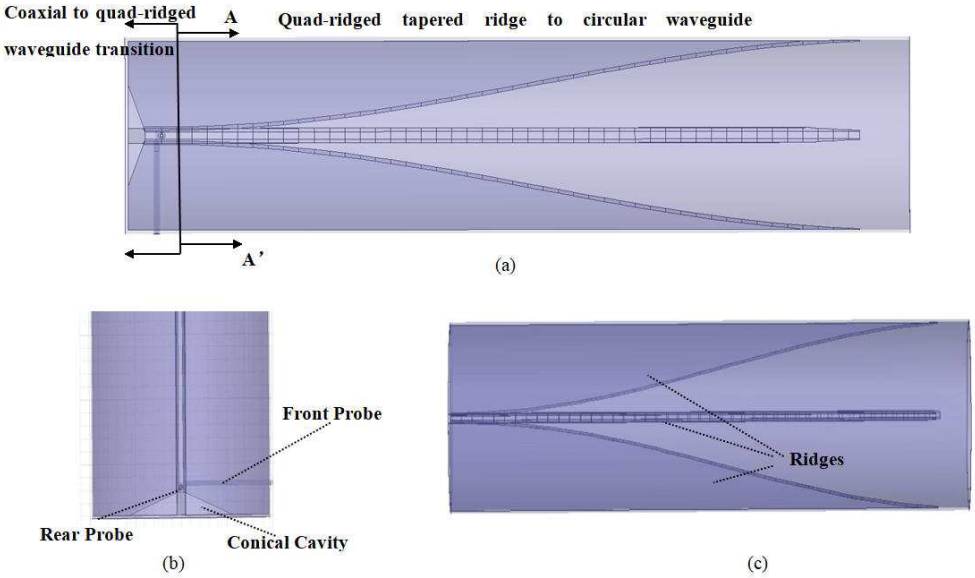

Fig. 2 QRWG OMT Structure: (a) QRWG OMT model; (b) Coaxial to QRWG transition (the center conductor of each coaxial feed extends across the ridge gap and connecting to the opposing ridge); (c) quad-ridged tapered ridge to circular waveguide transition.

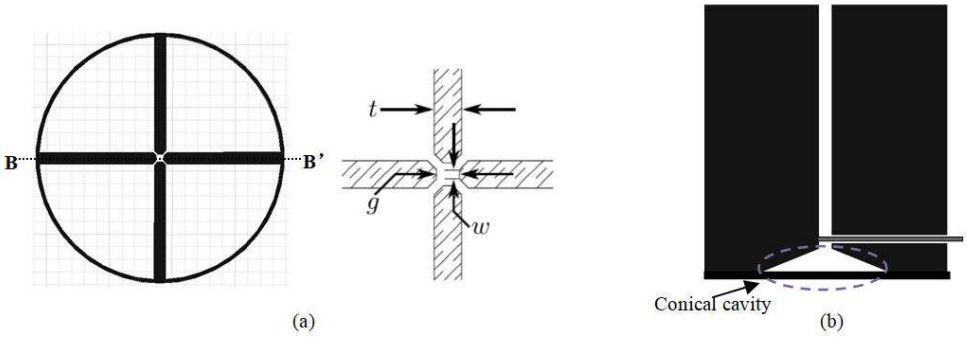

Fig. 3 Coaxial to quad-ridged waveguide transition: (a) Cross section of quad-ridged waveguide; (b) Side view of the ridges ended with the conical cavity.

circular waveguide largely determines the cut-off frequency of TE21L. For single-mode operation, the increase of the bandwidth between the TE11 and the TE21L modes and the impedance matched to the impedance of coaxial cable can be obtained by loading ridges with a very small gap. The QRWG at the coaxial transition consists of a 45-degree ridge chamfer with a flat surface in the center, which enables the gaps between the four ridges to be sufficiently small to have a nearly constant impedance values over the operational frequency range.

At the same time, the way to terminate the back cavity of the waveguide is very critical. The short circuit following the termination of the ridges is shown in Figure 3(b) to be in the shape of a 135-degree conical cavity. It was found that this geometry gives better impedance performance than a flat back cavity and can be seen as a matching section from short end to open end (near the coaxial probe). The radius and height of the conical cavity are such that no modes propagate past the ends of the ridges. In order to match the 50-Ohm coaxial line, initial values of the cone height and radial size as well as location of coaxial probes can be determined.

Figure 5(a) plots characteristic impedance of QRWG and reflection coefficient of coaxial to quad-ridged waveguide transition at L-band with diameter of circular waveguide d of 192 mm as well as parameters of t, w and g of 9.4 mm, 4.4 mm and 6 mm respectively. The end of four ridges is truncated by a conical cavity with a radius of 57 mm and height of 18 mm. At 0.8 GHz and 2.2 GHz, the characteristic impedance of QRWG is 49.9 Ohm and 48.3 Ohm for the dominant modes, respectively. From 0.9 to 2 GHz a return loss better than 20 dB can be achieved for this coaxial to quad-ridged waveguide transition. For S-band, diameter of circular waveguide d and parameters of t, w and g are 116, 9.5, 4.5 and 6 mm respectively and the end of four ridges is truncated by a cone with a radius of 30 mm and height of 12 mm. Figure 5(b) plots characteristic impedance of QRWG section as well as return loss of coaxial to quad-ridged waveguide transition. At 1.5 GHz and 3.5 GHz, the quad-ridged waveguide impedance is 51.6 Ohm and 50.3 Ohm for the dominant modes, respectively. From 1.5 to 3.4 GHz a return loss better than 20 dB can be achieved for this coaxial to quad-ridged waveguide transition.

2.2.2 Design of quad-ridged to circular waveguide transition

The quad-ridged to circular waveguide taper profile is designed to provide a smooth impedance transition from the chamfered quad-ridged waveguide at the coaxial transition to the circular waveguide near the OMT input. Three types of tapered lines are commonly used for matching transformer transitions: exponential taper, triangular taper and Klopfenstein taper. The Klopfenstein impedance taper has been shown to be the best in the sense that the reflection coefficient is the lowest over the pass band, and the second is the triangular taper. However, there exist steps at the ends of the Klopfenstein tapered section, so the taper cannot smoothly join the source and load impedances (Villiers et al. 2008). In this design we choose the triangular taper for the ridges' profile inside the waveguide, as seen in Figure 6(a), and the function of the taper profile is as follows:

$$x = (d - g)/2 \times \sin^m(\pi \times z/2/l) \tag{1}$$

with parameters m and l, where l is the length of the tapered ridge section.

The ridge profiles with different values of m are shown in Figure 6(b). In Equation (1), l is chosen as 850 mm and 450 mm for L-band and S-band respectively and then an optimal value of m is determined for the best and most smooth reflection coefficient curve. In Figure 6(c), the reflection coefficients for different values of m from 1.2 to 2.8 are given in the frequency range of 0.8–2.2 GHz for L-band quad-ridged to circular waveguide transition. The position of the first dip of the reflection coefficient (at about 0.9 GHz as shown in Fig. 6(b)) is determined by the waveguide's cut-off frequency and the overall taper length. With the increase of m from 1.2 to 2, the overall reflection coefficient becomes lower. As m increases to 2.4, ripples appear at the high frequencies and when m increases to 2.8, the return loss level increases slightly with the ripples still existing in the high frequency. In our design, the value of m from 2 to 2.4 will be suitable for the taper function and m value of 2 has been chosen considering the compromise of the better and smoother reflection coefficient curve achieved.

2.2.3 Overall optimization

Combining the two aforementioned components into a single HFSS model yields the overall simulated performance from the circular waveguide input to the coaxial output. In this section, we will take the proposed L-band OMT as an example. Full wave simulation analysis of two orthogonal polarization ports with normal probes (as shown in Fig. 7(a)) has been carried out. As can be seen in Figure 7(c), the simulated OMT performance for x polarization meets the –20 dB reflection coefficient specification from 0.95 GHz to 1.9 GHz. Because of the different location of the probe for y polarization, the simulated OMT performance for y polarization meeting the –20 dB reflection specification only ranges from 1.02 GHz to 1.67 GHz,

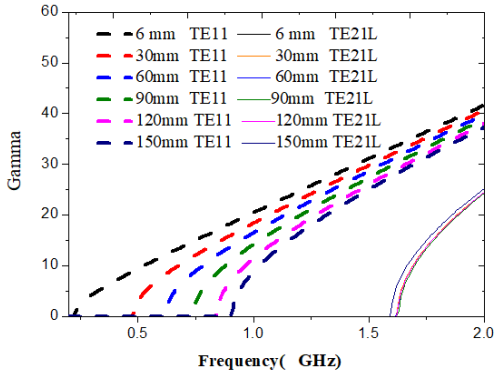

Fig. 4 The propagation constants of TE11 mode and TE21L mode in QRWG with different gap width g.

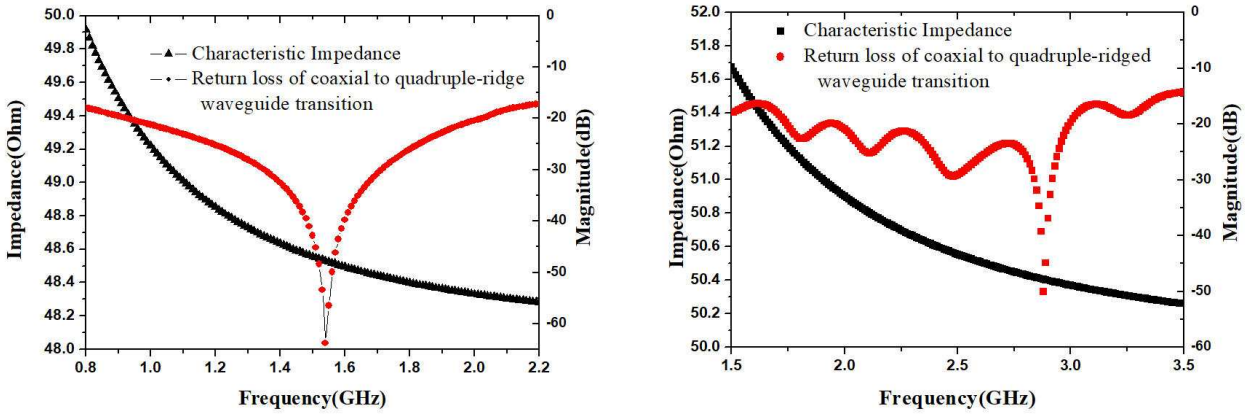

Fig. 5 Characteristic impedance of the QRWG and return loss of coaxial to quad-ridged waveguide transition (a) L-band (b) S-band.

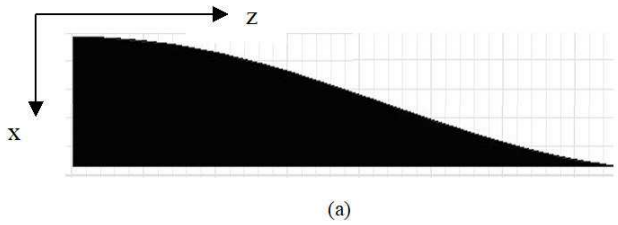

(a)

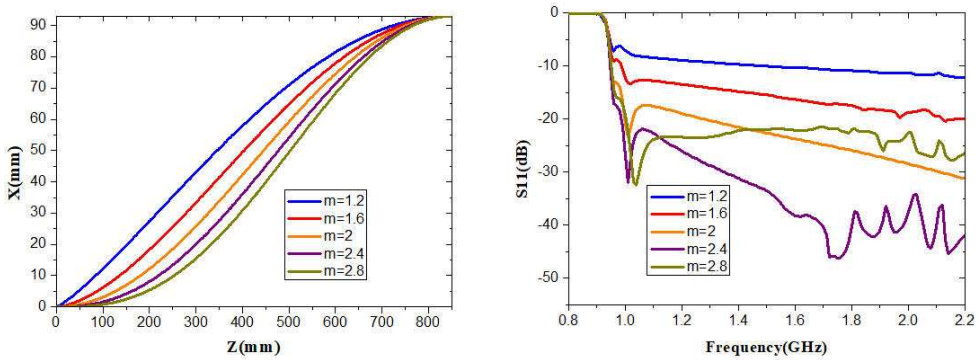

(b) (c)

Fig. 6 Quad-ridged to circular waveguide transition. (a) Side view of tapered ridge. (b) Ridge profile with different values of m. (c) Reflection coefficient versus frequency with different values of m.

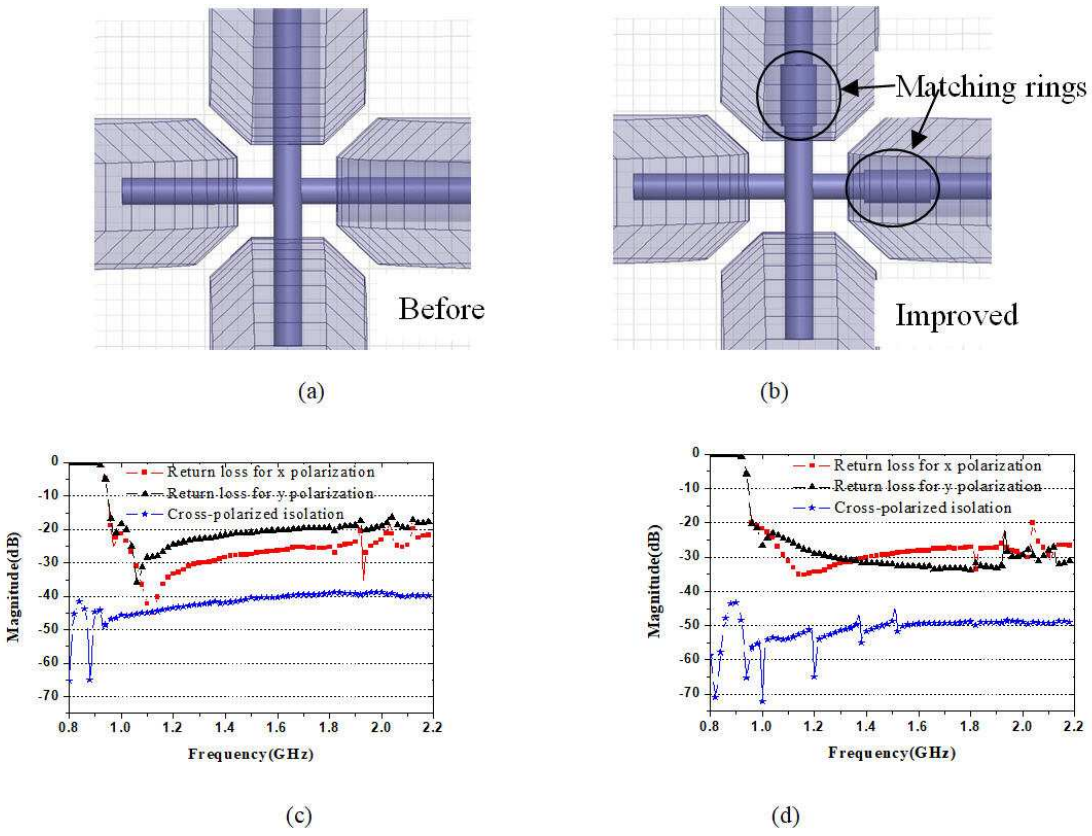

Fig. 7 (a) Structure of original OMT with normal probes. (b) Structure of improved OMT with matching rings into the probes. (c) Full wave simulation of two orthogonal polarization ports for original OMT. (d) Full wave simulation of two orthogonal polarization ports for improved OMT.

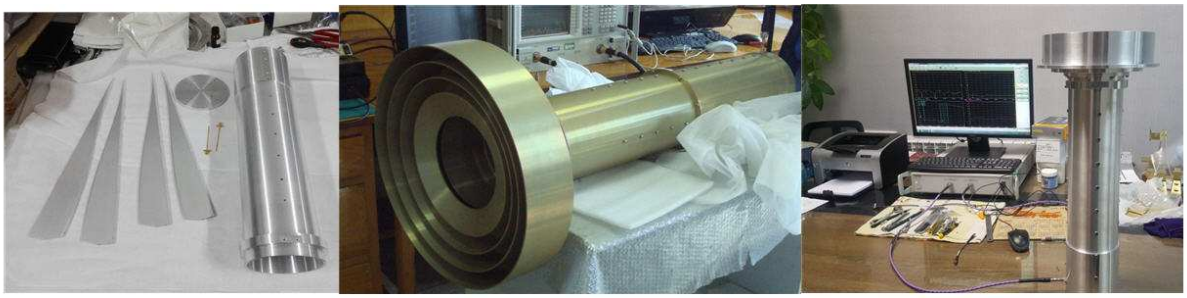

Fig. 8 (a) Components of the QRWG OMT. (b) L-band OMT prototype connected with a corrugated horn for measurement. (c) S-band OMT prototype connected with a corrugated horn for measurement.

and the cross-polarized isolation between orthogonal polarizations is less than 40 dB at the high frequencies.

To improve the performance for y polarization and the isolation between two orthogonal ports, a matching ring is introduced (as seen in Fig. 7(b)). Figure 7(d) shows the HFSS simulated reflection coefficient of the L-band QRWG OMT with the matching rings at the two orthogonal coaxial ports as well as the cross-polarized isolation. It can be seen that the simulated OMT performance for y polarization has been improved significantly, with –20 dB reflection coefficient and the isolation higher than 45 dB from 0.95 GHz to 1.95 GHz. The simulated response meets the specification with a large margin. The same optimization process can be applied in the QRWG OMT design at S-band and we will not repeat the design for brevity.

2.3 L- and S-band Prototype Measurement

The optimized QRWG OMTs at L- and S-bands have been manufactured. Figure 8(a) shows the components of the QRWG OMT, including four ridges, one bottom plate, two probes and the outer cylinder of the circular waveguide.

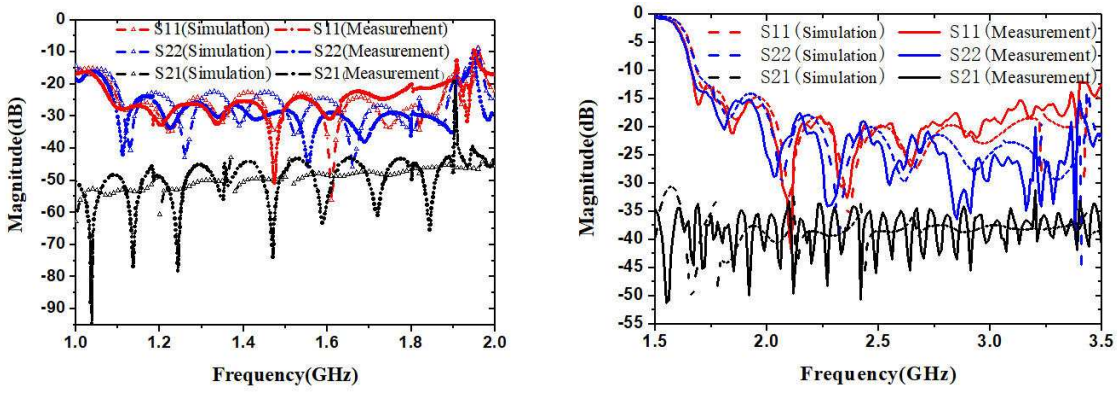

(a) (b)

Fig. 9 Simulation and measurement of L- and S-band QRWG OMT connected with a corrugated horn: (a) S-parameters at L-band; (b) S-parameters at S-band.

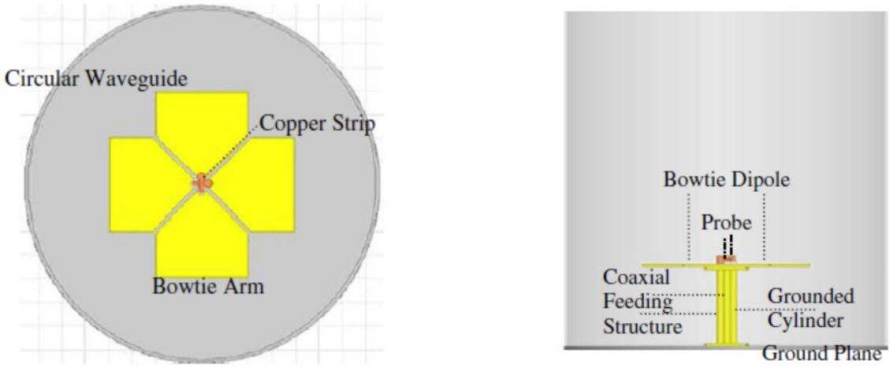

(a) (b)

Fig. 10 Structure of the purely metallic bowtie dipole OMT: (a) Top view; (b) Side view.

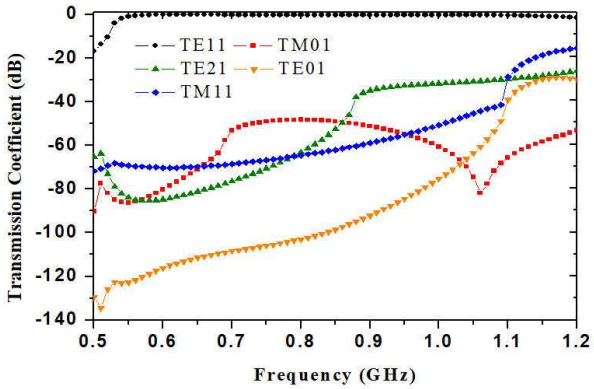

Fig. 11 Transmission coefficient from TEM mode of coaxial port to the first five modes of circular waveguide port.

The L- and S-band QRWG OMTs are constructed from aluminum, with the outer shape of the waveguide machined and the ridges laser-cut as separate pieces.

Figure 9 shows the HFSS simulated and measured results of reflection coefficient and cross-polarized isolation at two orthogonal coaxial ports for the L- and S-band OMTs connected with a corrugated horn, where the measurements are obtained using an Agilent E5071C ENA Series network analyzer as seen in Figure 8(b) and Figure 8(c). As can be seen in Figure 9, the measured results agree well with the simulated for L-band and S-band OMTs. The measured reflection coefficient of the L-band OMT is below –20 dB and the cross-polar isolation is higher than 40 dB from 1.2 GHz to 1.8 GHz. The per-

(a) (b) (c)

Fig. 12 (a) Feeding structure of bowtie dipole part with a ground plane. (b) P-band bowtie dipole OMT structure. (c) Bowtie dipole OMT under test.

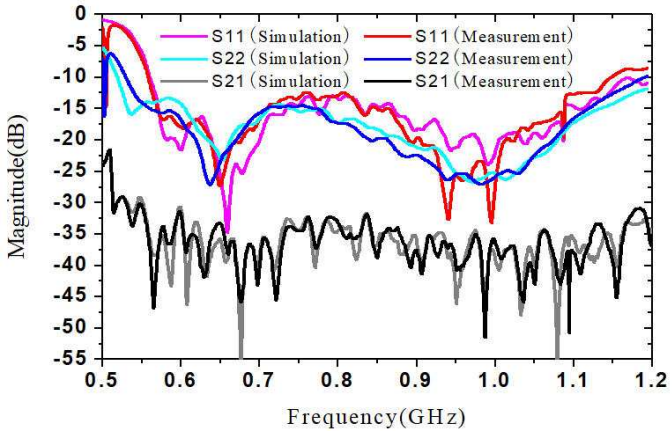

Fig. 13 Simulation and measurement of P-band bowtie dipole OMT.

formance is limited by the corrugated horn working from 1.2 GHz to 1.8 GHz. The reflection coefficient of S-band OMT is lower than –18 dB and the isolation is higher than 35 dB from 2 GHz to 3 GHz with low-frequency performance limited by waveguide cut-off and the total length, and high-frequency performance limited by the TE21L trapped-mode resonances.

3 DEVELOPMENT OF THE NOVEL BOWTIE DIPOLE OMT AT P-BAND

The OMTs at L- and S-band are designed based on circular QRWG type. However the QRWG OMT will require a length more than 1 m for 0.56–1.12 GHz frequency range, which corresponds to a huge mass and very large dewar size. Planar OMTs (Grimes et al. 2007) have a very compact size with a single mode bandwidth of 1.6:1, but 180° hybrids and supporting dielectric substrates are needed leading to additional loss and therefore increasing the system noise. The dipole OMTs (Lehmensiek & Theron 2014, Lehmensiek & Theron 2011) are very compact and can be of pure metal structure. However, the bandwidth of reported dipole OMT is not more than 1.7:1, which does not meet the octave bandwidth requirement of FAST P-band receiver system. In order to broaden the bandwidth of the dipole OMT, a compact wideband bowtie dipole is introduced into a circular waveguide as the feeding structure (Fan et al. 2019). The symmetrical structure and center feeding structure of the bowtie dipole OMT increase single mode bandwidth and guarantee no trapped mode generated. This novel bowtie dipole OMT for cryogenic octave bandwidth (0.56–1.12 GHz) receiver system of FAST at P-band has good electric properties with a very short length of only 300 mm (smaller than one wavelength of the center frequency).

3.1 Structure and Working Principle

Figure 10 shows the geometry of the bowtie dipole OMT at P-band, composed of a circular waveguide, a pair of crossed bowtie dipoles, a ground plane, two grounded posters and two coaxial (air filled) feeding structures with outer conductors grounded and inner conductors (probes) connected to the opposite metallic arm plate via copper strips at one end, and connected to Small A Type (SMA) connectors underneath the ground at the other end.

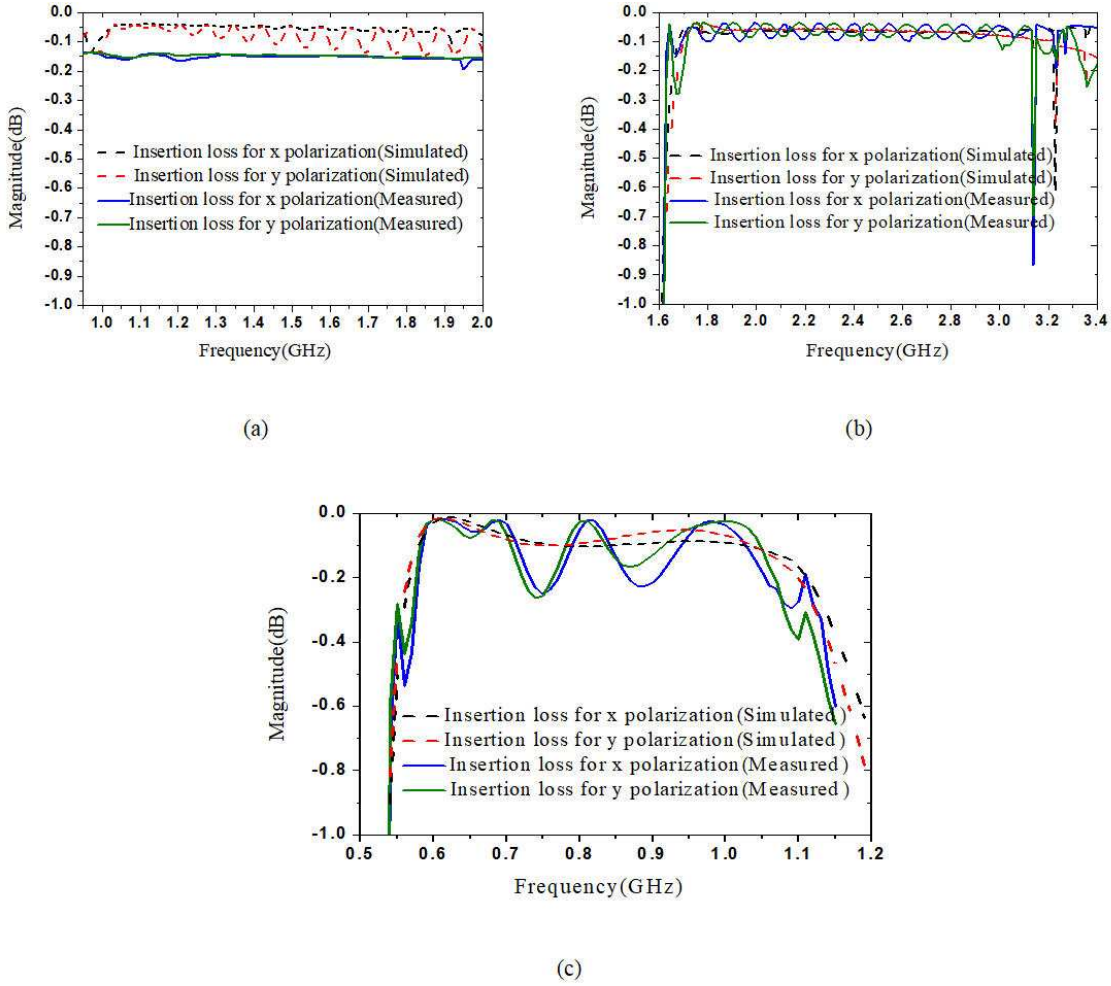

Fig. 14 Simulated and measured insertion loss for FAST OMTs at room temperature: (a) L-band; (b) S-band; (c) P-band.

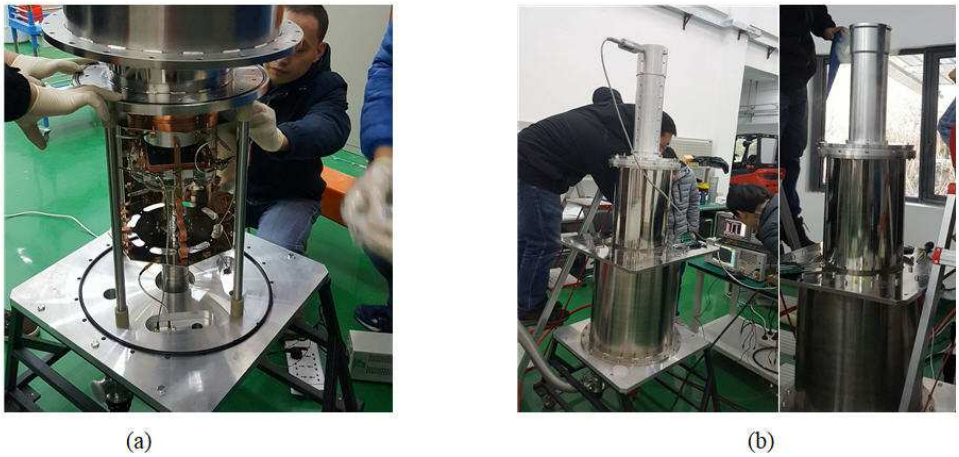

Fig. 15 FAST Cryogenic Receiver System: (a) Receiver front-end structure in the dewar; (b) Y-factor noise measurement.

Then, single-end LNAs can be connected directly to the OMT. In a circular waveguide, the theoretical maximum pure single-mode bandwidth is 1.31:1, limited by the first higher-order mode TM01. Therefore, in order to increase the single-mode bandwidth in practice, the excitation to the waveguide should be in such a way that all higher-order modes are not excited. By the proposed bowtie dipole feeding in this OMT, the electrical field distribution has a good symmetry with electric field line starting from one patch and terminating at the opposite as well as relatively strong

electric field at the axial direction line, which allows the existence of the TE11 and TM11 modes. However, TM01, TE21 and TE01 modes with zero E-field at the cross section center are not excited since these modes cannot satisfy the properties of the bowtie dipole electrical field distribution. Therefore, the single-mode bandwidth of the proposed OMT is determined by the cut-off frequencies of the fundamental mode TE11 and the higher-order mode TM11, for the low end and the high end of the band, respectively, with a value of 2.08:1.

3.2 Design Principle

A circular waveguide with a radius of 170 mm is chosen in order to have the same dimension as the horn waveguide used for the FAST dish. Then, the single-mode bandwidth of TE11 is from 0.52 GHz to 1.08 GHz, which is a bit different from the required band of 0.56–1.12 GHz. The reasons for this choice of the waveguide dimension, in addition to the size of horn waveguide, are: i) With the cut-off frequency of TE11 mode at 0.52 GHz, we have a margin to the low end of our operating band of 0.56–1.12 GHz so the reflection coefficient can achieve to be below –10 dB; ii) Even the cut-off frequency of TM11 mode is at 1.08 GHz, the upper band edge 1.12 GHz is very close to the cut-off frequency and the transmission coefficient from coaxial TEM mode at the coax port to TM11 mode at the waveguide port is under –20 dB, as shown with the simulation results in Figure 11 transmission coefficients from the coaxial input port with the TEM mode to the first five modes in the circular waveguide port (defined as a multimode port) have been simulated using Ansys HFSS and shown in Figure 11(a). As expected, transmission coefficients from the TEM mode to TM01, TE01 and TE21 mode are extremely low, below –50 dB at low frequencies and –30 dB at the high frequencies, which means these higher-order modes have not been excited by this tight bowtie dipole geometry.

3.3 P-band OMT Prototype Measurement

The prototype of P-band bowtie dipole OMT is manufactured with the computer numerical controlled (CNC) machining on aluminium material. It is composed of four metal bowtie arms, two through-hole cylindrical coaxial outer conductors, two grounded cylinders, two coaxial inner probes and two feeding connectors as shown in Figure 12(a) and 12(b). Each part is processed and assembled separately. Considering the stability of the structure, there is a triangular base at the top and bottom of the grounded cylinder and the through-hole cylinder. There are two screw holes in each base connecting to the ground and the metal bowtie arm. One end of the coaxial inner probe is connected with an SMA connector, which penetrates through the ground into the inside of the hollow cylindrical coaxial outer conductor, and the other end is screwed into the feeding connector with the threaded hole. The other side of the feeding connector is screwed into the metal bowtie arm connecting to the grounded cylinder. S-parameters of P-band bowtie dipole OMT are measured by an Agilent E5071C ENA Series network analyzer as shown in Figure 12(c). Figure 13 shows the simulated and measured results of the reflection coefficients and the mutual coupling between the two orthogonal coaxial ports. The measurement agrees well with the simulation, showing the reflection coefficient and the mutual coupling below –10 dB and –30.5 dB respectively over 0.56–1.12 GHz. As predicted, no resonances of the trapped modes can be observed in the operating band.

4 NOISE ANALYSIS FOR OMTS PROPTOTYPE AND RECEIVER SYSTEM

Insertion loss can be measured by two methods: one is from the measured transmission coefficient of two OMT units connected back-to-back and the other is from the reflection coefficient of a single OMT with waveguide port shorted. Figure 14 shows the HFSS simulated and measured insertion loss for FAST L-, S- and P-band OMTs at room temperature. As expected, the measured insertion loss is higher than the ideal simulated values due to the surface roughness, the material ohmic loss and processing errors. Resonances can be seen in the operational band because of the closed cavity structure under test. The maximum measured insertion loss value is 0.2 dB or better across the entire band for L- and S-band QRWG OMTs which can be seen in Figure 14(a) and 14(b). The OMTs are cooled to approximately 70 K, which implies a predicted noise contribution less than 3.3 K. The measured maximum insertion loss of P-band OMT is above 0.5 dB at the low frequency, which agrees with the simulated data as shown in Figure 14(c). In fact, the main part of the measured insertion loss is due to the reflection effect, while the ohmic loss of this pure metal OMT is extremely low, which can be obtained by $-10 \times \log[|S21|^2 / (1 - |S11|^2)]$ with the maximum value of 0.15 dB and the average over the band below 0.05 dB. Internal structure and Y-factor noise measurement of FAST Cryogenic Receiver System are shown in Figure 15. Preliminary test results show the receiver system temperature at L, S and P bands below 10 K, 18 K and 28 K, respectively.

5 CONCLUSIONS

Design and development of wideband OMTs are presented for FAST cryogenic receiver systems at L- S- and P-band.

By designing two critical OMT parts separately, FAST L- and S-band QRWG OMTs are developed and design scenario includes appropriate design of QRWG cross section and the way to terminate the back of the waveguide in the coaxial to quad-ridged waveguide transition, and the parameter selection of the curve function for quad-ridged to circular waveguide transition as well as the design of improved probes. Excellent in-band performance of 18 dB return loss and –35 dB cross-coupling are realized for FAST L- and S-band QRWG OMT with insertion loss below 0.2 dB, corresponding to a noise contribution less than 3.3 K. The design ideas can also be applied to QRWG OMT design for other frequency ranges. For FAST P-band, a novel wideband bowtie dipole OMT is proposed with a length of 300 mm, only 0.56 wavelengths at the low-end frequency of 0.56 GHz. The single mode bandwidth of bowtie dipole OMT has been achieved to 2.08:1. Measurements showed a reflection coefficient below –10 dB for both polarizations, cross-coupling levels below –30.5 dB and transmission coefficient above –0.5 dB over the operating band of 0.56–1.12 GHz. The purely metallic bowtie dipole OMT is very compact, easy to fabricate and therefore, an excellent candidate for low frequency, high sensitivity, cryogenic integration and miniaturization application.

Acknowledgements This work was supported by Joint Research Fund in Astronomy (U1931129, U1631115 and U1831117) under cooperative agreement between the National Natural Science Foundation of China (NSFC) and the Chinese Academy of Sciences, NSFC-STINT Grant of 11611130023 (CH2015-6360), and the NSFC (Grant Nos. 11403054 and 11973006).

References

Boifot, A. M., Lier, E., & Schaug-Pettersen, T. 1990, in IEE Proceedings H - Microwaves, Antennas and Propagation, 137, 396

Coutts, & M., G. 2011, IEEE Transactions on Antennas & Propagation, 59, 1910

Fan, J., Yan, Y., Jin, D., & Luo, J. R. 2017, Progress In Electromagnetics Research C, 72, 115

Fan, J., Zhu, K., Yang, J., & Yan, Y. 2019, Microwave and Optical Technology Letters, 61, 883

Grimes, P. K., King, O. G., Yassin, G., & Jones, M. E. 2007, Electronics Letters, 43, 1146

Lehmensiek, R., & Theron, I. P. 2011, IEEE Transactions on Antennas & Propagation, 59, 1894

Lehmensiek, R., & Theron, I. P. 2014, in The Design of the MeerKAT UHF Band Feed, the 8th European European Conference on Antennas & Propagation

Nan, R. 2006, Science in China Series G, 49, 129

Reck, T. J., & Chattopadhyay, G. 2013, IEEE Microwave & Wireless Components Letters, 23, 569

Robertson, S. 1956, Ire Transactions on Microwave Theory & Techniques, 4, 263

Stennes, M. 2000, L-Band OMT Test Report, *https://www.gb.nrao.edu/electronics/edir/edir245.pdf*

Skinner, S. J., & James, G. 1991, IEEE Transactions on Microwave Theory & Techniques, 39, 294

Villiers, D. I. L. D., Meyer, P., & Palmer, K. D. 2008, Electronics Letters, 45, 60